Sound Radiation from a Subsonic Rotor Subjected to Turbulence

M. SEVIK

The Pennsylvania State University

The broadband sound radiated by a subsonic rotor subjected to turbulence in the approach stream has been analyzed. The power spectral density of the sound intensity has been found to depend on a characteristic time scale—namely, the integral scale of the turbulence divided by the axial flow velocity—as well as several length-scale ratios. These consist of the ratio of the integral scale to the acoustic wavelength, rotor radius, and blade chord. Due to the simplified model chosen, only a limited number of cascade parameters appear. Limited comparisons with experimental data indicate good agreement with predicted values.

The noise radiated by rotating machinery is known to consist of a broadband, random signal on which are superimposed a number of discrete peaks. These characteristics of the radiated noise spectrum have been observed on a wide range of turbomachinery such as aircraft compressors (refs. 1, 2, 3), turbines (ref. 4), fans (ref. 5), and marine propulsors.

The discrete peaks, which are due to mutual interference effects between blade rows, were of greatest concern as a cause of public annoyance and were the first to be investigated (refs. 6, 7, 8). This source of sound is now well understood and its reduction has met with a certain measure of success (ref. 10).

Broadband radiation has received relatively little attention in aircraft applications. The vibratory forces generated by turbulence, however, were of considerable interest in certain naval applications since marine propellers operate well within the boundary layer of a ship's hull. In this case, the length scales of the turbulence and the propeller are of comparable magnitudes, and, hence, strong thrust and torque fluctuations can arise (ref. 11).

The random pressure fluctuations within a turbomachine which give rise to broadband radiation are due to the following phenomena:

(1)   Turbulence in the approach stream generated, for instance, by upstream blade rows or by the combustion system.

(2)   Boundary layer turbulence at the duct walls.

(3)   Vortex shedding from the blade trailing edges.

(4)   Random variations of the tip vortex strength.

Sharland (ref. 5), Smith and House (ref. 3), and Smith and Bushell (ref. 4) conclude from their measurements that the major source of broadband, random noise in compressors and turbines is turbulence in the approach stream. This has also been found to be the case in marine propulsors (ref. 11), although vortex shedding from the blade trailing edges can—under certain conditions—become the dominant source over a range of frequencies.

In this paper, the sound radiated from a rotor subjected to turbulence in the approach stream, at subsonic speeds, will be considered.

CORRELATION OF PRESSURE FLUCTUATIONS

Curle (ref. 12) and Doak (ref. 13) have shown that the dipole radiation from a turbulent flow containing rigid surfaces can be expressed in terms of the distribution of fluctuating pressures acting over the surfaces. In order to calculate the characteristics of these pressures, imagine the rotor blades to be subdivided into an arbitrarily large number of surface elements. The fluid velocity is measured with respect to a coordinate system α' ($\alpha' = 1', 2', 3'$) that is fixed in space (fig. 1). An unprimed system α ($\alpha = 1, 2, 3$) is fixed to the rotor and is so oriented that one of its axes coincides with the centerline of the rotor shaft.

The time-dependent pressures acting on the various surface elements are related by virtue of spatial and temporal correlation of the velocity fluctuations in the approach stream as well as by virtue of induction effects that take place between adjacent blade elements. The acoustic radiation depends on the correlation area for the pressure-difference fluctuations; because of induction effects this area may differ considerably from the correlation area of the turbulence.

Since the physical quantities involved in this problem are tensors, the index notation—including the summation convention in the case of repeated indices—constitutes the most convenient choice. Superscripts are used to denote the direction along one of the coordinate axes, whereas subscripts are used to denote the rotor blade element involved. For example, $u_k^\beta(\tau')$ denotes the component of the fluctuating velocity at time τ' in the direction β of the rotating reference frame at the blade element k. Similarly, $F_{ik}^{\alpha\beta}(t,\tau')$ denotes the aerodynamic force acting on the ith blade element in the direction α at the instant of time t caused by a velocity fluctuation of unit magnitude in the direction β to which the kth
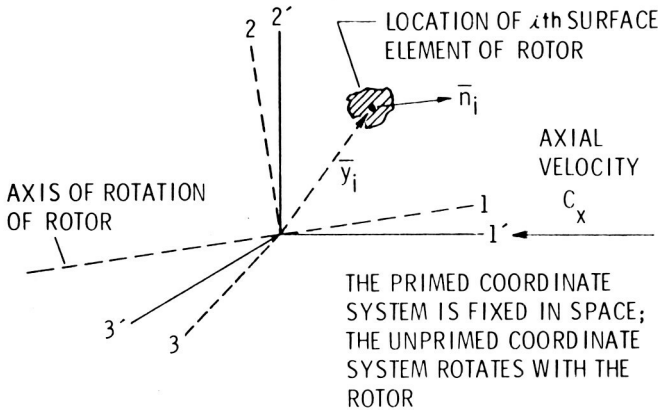
FIGURE 1.—*Coordinate system.*

blade element was subjected at the instant of time τ'. Finally, $\ell_i{}^\alpha(t)$ indicates the aerodynamic force acting on the ith blade element at time t in the direction α. In terms of these quantities, and neglecting higher order terms, the lift force is given by

$$\ell_i{}^\alpha(t) = \int_{-\infty}^{t} F_{ik}{}^{\alpha\beta}(t,\tau') u_k{}^\beta(\tau') \, d\tau' \tag{1}$$

where

$$\alpha, \beta = 1, 2, 3$$
$$i, k = 1, 2, \ldots n$$

with

$$\tau' \leq t$$

In most cases, the aerodynamic force tensor is time-invariant, and equation (1) can be written as a convolution integral:

$$\ell_i{}^\alpha(t) = \int_0^{\infty} F_{ik}{}^{\alpha\beta}(t) u_k{}^\beta(t-\tau) \, d\tau \tag{2}$$

where

$$\tau = t - \tau' \geq 0$$

Since the aerodynamic forces $\ell_i{}^\alpha(t)$ are random functions, they are determined statistically by the complete system of joint-probability distributions of the values of the functions at any n values of t, where n may take any integral value. From an engineering standpoint, the correlation tensor $\langle \ell_i{}^\alpha(t) \ell_j{}^\beta(t+\tau) \rangle$ and its Fourier transform are the most significant quantities. In forming average values of the forces and fluid velocities,

we assume that the random processes are stationary and ergodic. The mathematical expectation

$$
\begin{aligned}
E[\ell_i{}^\alpha(t)\ell_j{}^\beta(t+\tau)] &= \lim_{T\to\infty}\frac{1}{T}\int_0^T \ell_i{}^\alpha(t)\ell_j{}^\beta(t+\tau)\ dt \\
&= \Phi_{\ell i \ell j}^{\alpha\beta}(\tau)
\end{aligned}
\tag{3}
$$

can be expressed in terms of the aerodynamic force functions and the velocity fluctuations in the form

$$
\begin{aligned}
\Phi_{\ell i \ell j}^{\alpha\beta}(\tau) &= \int_0^\infty F_{ik}{}^{\alpha\gamma}(\tau_1)\ d\tau_1 \int_0^\infty F_{jr}{}^{\beta\delta}(\tau_2)\ d\tau_2 \\
&\quad \times \lim_{T\to\infty}\frac{1}{T}\int_0^\infty u_k{}^\gamma(t-\tau)u_r{}^\delta(t+\tau-\tau_2)\ dt \\
&= \int_0^\infty F_{ik}{}^{\alpha\gamma}(\tau_1)\ d\tau_1 \int_0^\infty F_{jr}{}^{\beta\delta}(\tau_2)\ d\tau_2 R_{kr}{}^{\gamma\delta}(\tau)
\end{aligned}
\tag{4}
$$

$R_{kr}{}^{\gamma\delta}(\tau)$ is the velocity correlation tensor for the points located at $\mathbf{y}_k$ and $\mathbf{y}_r$, respectively. The spectrum tensor of the force fluctuations can now be found by taking the Fourier transform of the correlation tensor:

$$
\begin{aligned}
G_{\ell i \ell j}^{\alpha\beta}(\omega) &= \frac{1}{\pi}\int_{-\infty}^\infty \Phi_{ij}{}^{\alpha\beta}(\tau)[\exp i\omega\tau]\ d\tau \\
&= \int_0^\infty F_{ik}{}^{\alpha\gamma}(\tau_1)[\exp i\omega\tau_1]\ d\tau_1 \int_0^\infty F_{jr}{}^{\beta\delta}(\tau_2)\ [\exp(-i\omega\tau_2)]\ d\tau_2 \\
&\quad \times \frac{1}{\pi}\int_{-\infty}^\infty R_{kr}{}^{\gamma\delta}(\tau)[\exp(-i\omega\tau)]\ d\tau \\
&= [H_{ik}{}^{\alpha\gamma}(\omega)]^*[H_{jr}{}^{\beta\delta}(\omega)]G_{kr}{}^{\gamma\delta}(\omega)
\end{aligned}
\tag{5}
$$

where $H(\omega)$ represents the aerodynamic frequency response function, $G_{kr}{}^{\gamma\delta}(\omega)$ is the spectrum tensor of the turbulence, and $i=\sqrt{-1}$.

APPLICATION TO A ROTOR

As an illustration, consider a rotor placed in a flow containing homogeneous and isotropic turbulence. In this case, the velocity correlation tensor can be expressed in terms of the distance r between two points in the flow field and the mean square value of the velocity fluctuations u^2 as follows:

$$R_{kr}{}^{\alpha\beta}(r) = u^2 \left[-\frac{1}{2r} r^{\alpha} r^{\beta} \frac{\partial f}{\partial r} + \left(f + \frac{1}{2} r \frac{\partial f}{\partial r} \right) \delta^{\alpha\beta} \right] \tag{6}$$

where $\delta^{\alpha\beta}$ is the Kroenecker delta. The coefficient of longitudinal correlation f can be approximated by an exponential function; namely

$$f(r) = \exp\left(-\frac{r}{\Lambda_f} \right) \tag{7}$$

where Λ_f is the integral scale of the turbulence. Furthermore, the velocity correlation tensor is approximated by

$$R_{kr}{}^{\alpha\beta}(r) \cong \left[\exp\left(-\frac{q}{\Lambda_f} \right) \right] R_{kk}{}^{\alpha\beta}(c_x\tau) \tag{8}$$

where $q = |\mathbf{y}_k - \mathbf{y}_r|$ is the distance between blade elements k and r.

We now calculate the spectrum tensor of the force fluctuations normal to the plane of the rotor. In equation (5), α and β are both assigned the value 1, which corresponds to the direction normal to the rotor disk. The indices γ and δ take the values 1 and 2 only, since axis 3 coincides with the spanwise axis of a blade. From equation (8) the velocity correlation tensor has the components

$$
\left.
\begin{aligned}
R_{kr}{}^{11}(r) &= u^2 \exp\left\{ -\left(\frac{c_x\tau}{\Lambda_f} + \frac{q}{\Lambda_f} \right) \right\} \\[2mm]
R_{kr}{}^{22}(r) &= u^2\left(1 - \frac{1}{2}\frac{c_x\tau}{\Lambda_f} \right) \exp\left\{ -\left(\frac{c_x\tau}{\Lambda_f} + \frac{q}{\Lambda_f} \right) \right\} \\[2mm]
R_{kr}{}^{12}(r) &= R_{kr}{}^{21}(r) = 0
\end{aligned}
\right\} \tag{9}
$$

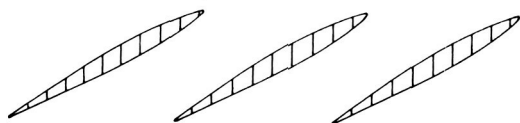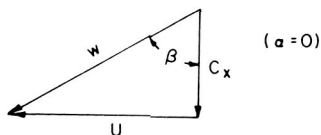where c_x is the axial velocity, as shown in figure 2.

FIGURE 2.—*Velocity diagram for an axial flow pump or compressor stage.*

The Fourier transforms of these correlation functions can readily be calculated:

$$
\left.
\begin{aligned}
G_{kr}{}^{11}(\omega) &= \frac{2}{\pi}\, u^2 \left[\frac{\dfrac{c_x}{\Lambda_f}}{\left(\dfrac{c_x}{\Lambda_f}\right)^2 + \omega^2} \right] \exp\left(-\frac{q}{\Lambda_f}\right) \\[2em]
G_{kr}{}^{22}(\omega) &= \frac{2}{\pi}\, u^2 \left[\frac{\dfrac{c_x}{\Lambda_f}}{\left(\dfrac{c_x}{\Lambda_f}\right)^2 + \omega^2} \right] \left\{ 1 + \frac{1}{2}\left[\frac{\left(\dfrac{c_x}{\Lambda_f}\right)^2 - \omega^2}{\left(\dfrac{c_x}{\Lambda_f}\right)^2 + \omega^2} \right] \right\} \exp\left(-\frac{q}{\Lambda_f}\right)
\end{aligned}
\right\} \quad (10)
$$

The spectrum tensor of the force fluctuations therefore reduces to

$$
\begin{aligned}
G_{l_i l_j}^{11}(\omega) &= [H_{ik}{}^{11}(\omega)]^* [H_{jr}{}^{11}(\omega)] G_{kr}{}^{11}(\omega) \\
&\quad + [H_{ik}{}^{12}(\omega)]^* [H_{jr}{}^{12}(\omega)] G_{kr}{}^{22}(\omega)
\end{aligned} \quad (11)
$$

The simplest expression for the aerodynamic response function is that of Sears (ref. 14). This expression is based on two-dimensional, incompressible, thin-airfoil aerodynamics and ignores mutual interference between blade elements. The task of establishing aerodynamic response functions for cascades is yet to be accomplished. Recent experiments that have been performed at Pennsylvania State University, however, show that strip theory gives satisfactory predictions providing the value of the local lift slope is appropriately corrected. This correction consists in replacing the value of the lift slope—which is equal to 2π in Sears' equation—by the steady-state local value. In terms of Sears function, the values of $H(\omega)$ are given by

$$
\left.
\begin{aligned}
H_{ii}{}^{11}(\omega) &= H_i(\omega)\, \sin^2 \beta_i \\
H_{ii}{}^{12}(\omega) &= \tfrac{1}{2} H_i(\omega)\, \sin 2\beta_i
\end{aligned}
\right\} \quad (12)
$$

where

$H(\omega)$ $2\pi \rho w b \delta r K(\kappa)$

$K(\kappa)$ Sears function

κ $\dfrac{\omega b}{w}$

$2b$ blade chord
δr spanwise distance along the blade
w relative fluid velocity
β angle between the flow relative to the blade and the axial direction, as shown in figure 2.

We can further simplify our final expression if $H(\omega)$ is chosen as the mean value for the entire blade span. In this case

$$\frac{1}{n^2}\sum_{i=1}^{n}\sum_{j=1}^{n}{}'H_i^*(\omega)H_j(\omega)\cong H^*(\omega)H(\omega)=\mid H(\omega)\mid^2\cong(2\pi w\rho b)^2\frac{1}{(1+2\pi\kappa)}\,\delta r_i\delta r_j$$

(13)

The spectrum of the total normal force driving the rotor can now be found from equation (11), using equations (10), (12), and (13). It has the form

$$G(\Gamma)=\pi(\rho c_x^2 R^2)^2\left(\frac{2bB}{R}\frac{u}{c_x}\right)^2\left(\frac{1}{1+\phi^2}\right)f(\Gamma)S\left(\frac{R}{\Lambda_f}\right)$$

(14)

where $\phi=c_x/U$ is the flow coefficient, B is the number of rotor blades, and u/c_x is the turbulence level in the approach stream.

The function $S(R/\Lambda_f)$ represents a "correlation area" and is given by

$$S\left(\frac{R}{\Lambda_f}\right)=\frac{1}{B^2R^2}\int\int\exp\left(-\frac{q}{\Lambda_f}\right)dr_i\,dr_j;\qquad q=\mid \mathbf{r}_i-\mathbf{r}_j\mid$$

(15)

The integration is performed from the hub radius r_h to the tip radius R. This function has been plotted in figure 3 for rotors having various numbers of blades and hub-to-tip ratios.

The frequency dependence of the total force driving the rotor is given by $f(\Gamma)$, which has the form

$$f(\Gamma)=\left(\frac{1}{1+e\Gamma}\right)\left(\frac{1}{1+\Gamma^2}\right)\left(C+\frac{1-\Gamma^2}{1+\Gamma^2}\right)$$

(16)

where

$$\Gamma=\frac{\omega\Lambda_f}{c_x}$$

$$e=\pi\frac{2b}{\Lambda_f}\cos\beta$$

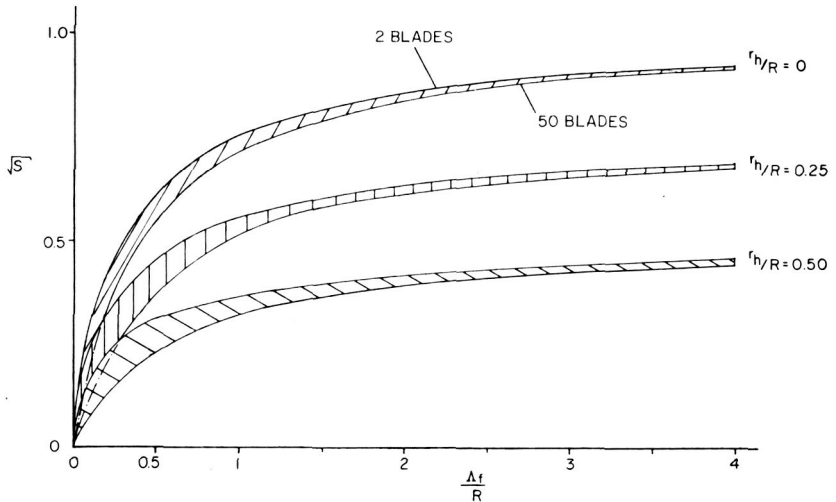$$C=2\left(1+\frac{1}{\phi^2}\right)$$

FIGURE 3.—"*Correlation area*" *in the spectrum function of the axial force.*

EXPERIMENTAL INVESTIGATIONS

To verify the theory, an experiment was conducted in the water tunnel of the Ordnance Research Laboratory at Pennsylvania State University (ref. 11). This tunnel has a test section that is 4 ft in diameter and 14 ft in length. Velocities as high as 80 fps can be achieved, and the static pressure can be varied from 3 to 60 psia. The settling section of the tunnel contains a honeycomb of large length-to-diameter ratio that reduces the turbulence level in the test section to about 0.1 percent.

A propeller was used for this investigation. The propeller had 10 blades with a constant chord length of 1 in. and a radius of 4 in. The design static thrust coefficient based on propeller disc area is 0.183, and the advance ratio at the design thrust coefficient is 1.17. The propeller and its installation in the water tunnel are shown in figure 4.

A special balance was designed for measuring the unsteady thrust force of the propeller. The arrangement used is shown in figure 5. A piezo-electric crystal is mounted in a steel cup at the end of the propeller shaft. After assembly, the cup is positioned by means of set screws until the hemispherical ball bonded to the crystal lies on the exact center line of the shaft, thus minimizing the crystal's response to bending distortions of the shaft caused by hydrodynamic moments acting on the propeller. The frequency response and the linearity of the balance are shown in figure 6.

During the tests, turbulence was generated by means of grids mounted 20 mesh sizes upstream of the propeller. Two grids were used with mesh
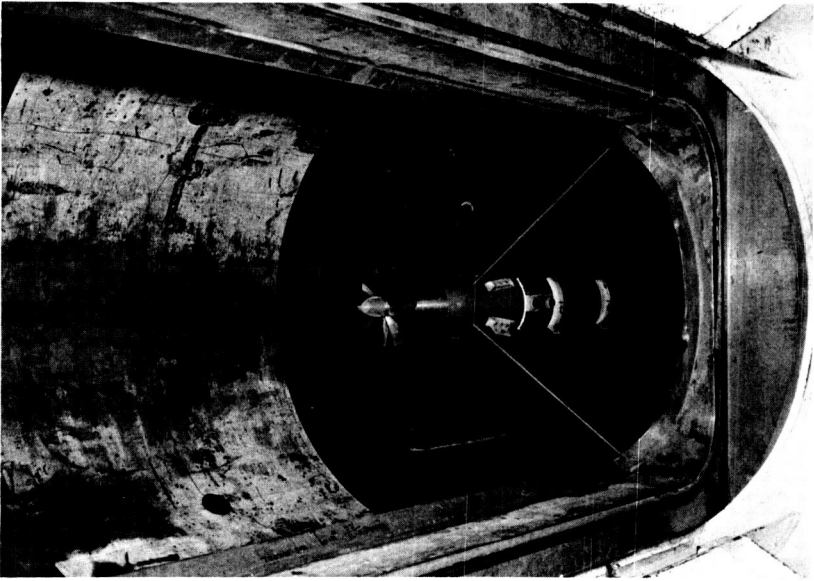
FIGURE 4.—*Experimental propeller and balance housing in the water-tunnel test section.*
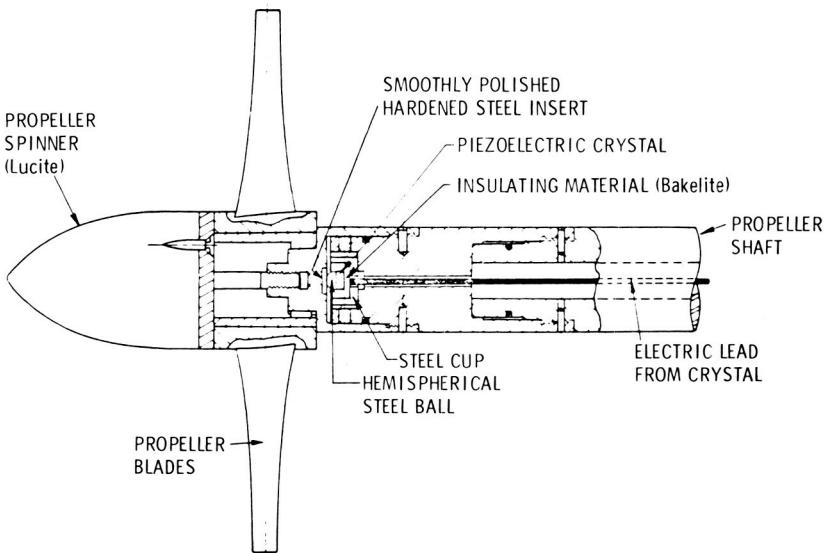
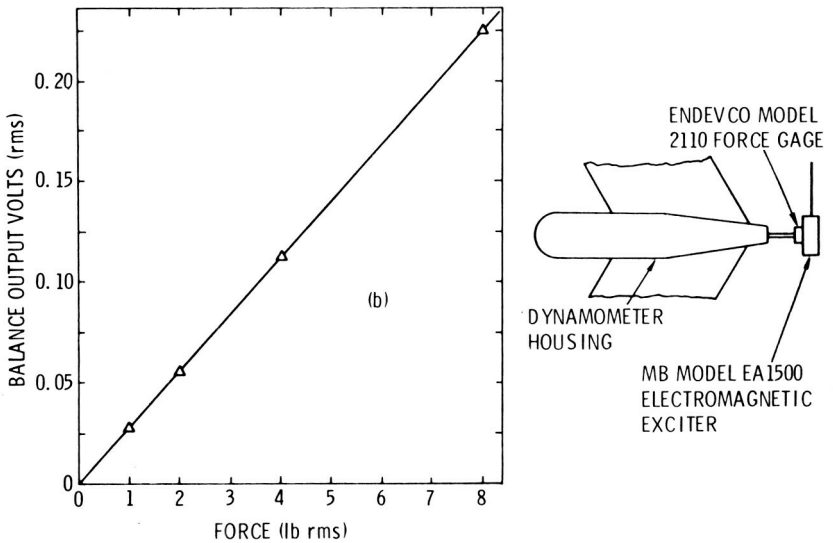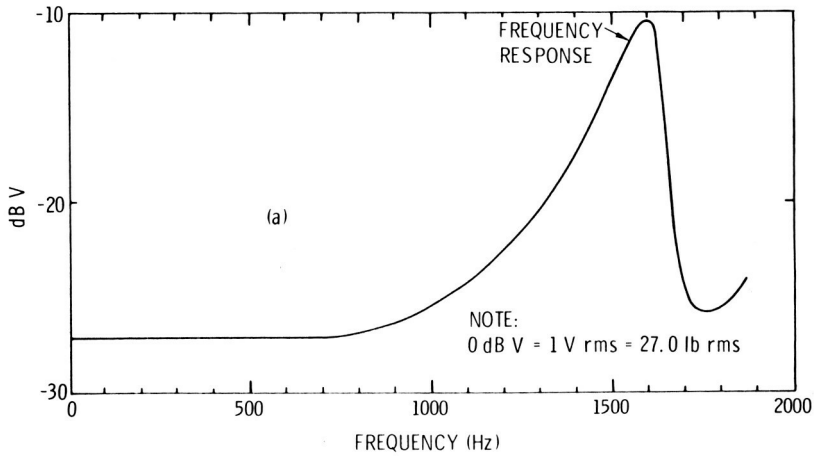

FIGURE 5.—*Unsteady force balance.*

FIGURE 6.—*Frequency response and linearity of balance.*

sizes of 4 in. and 6 in., respectively. The first had a solidity of 0.34 and was fabricated with $\frac{3}{4}$-in.-diameter rods. The second had a solidity of 0.27 and consisted of $\frac{7}{8}$-in.-diameter rods. Figure 7 shows a view of the propeller taken from a position upstream of the 4-in. grid in the water tunnel.

The measurements are compared in figure 8 with theoretical predictions. The "humps" in the measured spectrum occur at blade passage frequency.

FIGURE 7.—*Downstream view of propeller through the 4-inch grid.*

SOUND RADIATION FROM A ROTOR

The statistical measure of greatest engineering interest is the power spectral density of the sound pressure fluctuations. This is related to the power spectral density of the force fluctuations by a Green's function $g(\mathbf{x},\mathbf{y};\omega)$ as follows:

$$P(\mathbf{x};\omega) = \sum_{i=1}^{n} \sum_{j=1}^{n} g^*(\mathbf{x},\mathbf{y}_i;\omega)\, g(\mathbf{x},\mathbf{y}_j;\omega)\, G_{lil_j}^{11}(\omega) \tag{17}$$

If the rotor is housed in a duct, the radiation into the free field will be affected by the characteristics of sound propagation in the duct and by its intake geometry. These effects have been considered by Tyler and Sofrin (ref. 6), as well as by Morfey (ref. 15), for pure tone radiation.

In order to simplify the present problem, the Green's function chosen will be that of a dipole whose axis is normal to the rotor plane. Comparison of predicted acoustic power with experimental measurements on ducted fans will still be possible in cases where the dimension of the duct is comparable with, or greater than, the quarter wavelength of the sound generated. The appropriate Green's function for the far field is given by

$$g(\mathbf{x},\mathbf{y}_j;\omega) = -\frac{ik\,\cos\theta}{4\pi r}\{\exp ikr\}\{\exp[-ikr_j\,\cos(\varphi_j-\varphi)\,\sin\theta]\} \tag{18}$$

TEST No. 5531, RUN No. 2
DISTANCE BETWEEN GRID AND PROPELLER = 80 INCHES
WATER-TUNNEL TURBULENCE LEVEL WITHOUT GRID = 0.0011 U
TURBULENCE LEVEL AT PROPELLER DUE TO THE GRID = 0.03 U
TUNNEL VELOCITY = 15.4 ft/sec
PROPELLER ADVANCE RATIO = 1.22
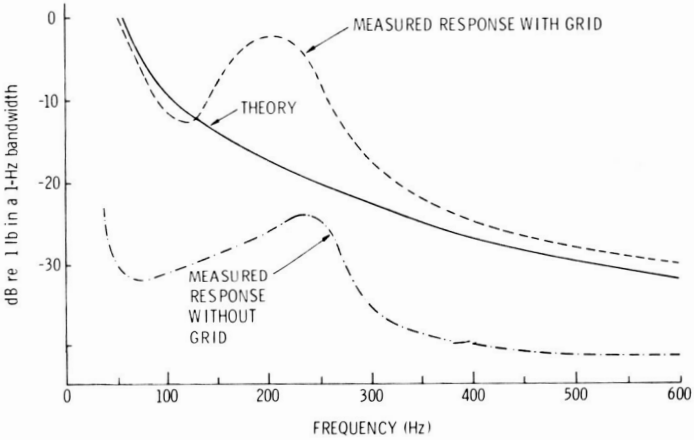
a.—*4-inch grid mesh.*

TEST No. 5530, RUN No. 2
DISTANCE BETWEEN GRID AND PROPELLER = 120 INCHES
WATER-TUNNEL TURBULENCE LEVEL WITHOUT GRID = 0.001 U
TURBULENCE LEVEL AT PROPELLER DUE TO THE GRID = 0.03 U
TUNNEL VELOCITY = 15.1 ft/sec
PROPELLER ADVANCE RATIO = 1.22
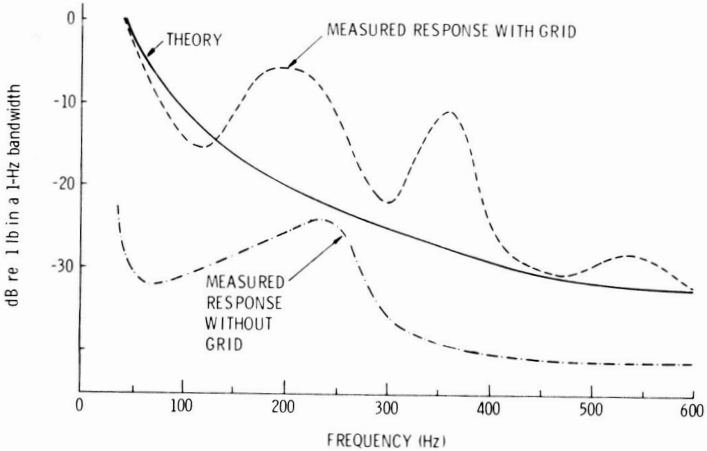
b.—*6-inch grid mesh.*

FIGURE 8.—*Power spectral density of the propeller response.*

where $k = \omega/c$. The polar coordinates used in this equation are defined in figure 9.

A further restriction is imposed by the requirement that the eddies be compact on a wavelength scale so that retarded time changes will be negligible. This implies that the acoustic wave length λ must be much larger than the integral scale Λ_f.

The spectral density of the sound intensity at $\mathbf{x}$ follows from equations (17) and (18):

$$I(\mathbf{x};\Gamma) = \frac{\pi^2}{4r^2} \left(\frac{u}{c_x}\right)^2 M^3 \left[1 - \left(\frac{r_h}{R}\right)^2\right]^2 \left(\frac{\rho c_x{}^3 R^2}{1+\phi^2}\right) \left(\frac{R}{\Lambda_f}\right)^2 g(\Gamma) F\left(\theta, \frac{R}{\Lambda_f}, kR\right)$$

(19)

where $M = c_x/c$ is the axial flow Mach number and $g(\Gamma) = \Gamma^2 f(\Gamma)$.

In deriving the function F, it is assumed that the solidity of the rotor is such that it can be treated acoustically as a disk. This implies that the acoustic wavelength must be much larger than the blade chord and the blade spacing. Under these conditions F has the form

$$F\left(\theta, \frac{R}{\Lambda_f}, kR\right) = \frac{\cos^2 \theta}{2\pi^2 \left[1 - \left(\frac{r_h}{R}\right)^2\right]^2 R^4} \int_{r_h}^{R} \int_0^{2\pi} \exp\left\{-\frac{R}{\Lambda_f}(Q^2 + Z^2)^{1/2}\right\}$$

$$\times \left[J_0(kRQ \sin \theta) + J_0(kRZ \sin \theta)\right] r_i\, dr_i\, d\varphi_i\, r_j\, dr_j\, d\varphi_j$$

(20)

where J_0 denotes Bessel functions and r_h denotes the hub radius. The quantities Q and Z are measured on the rotor disk and are given by

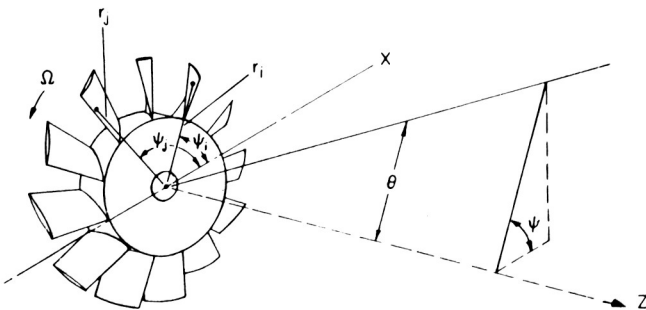$$Q = \frac{1}{R}(r_i \cos \varphi_i - r_j \cos \varphi_j)$$

FIGURE 9.—*Polar coordinate system.*

$$Z = \frac{1}{R} \left(r_i \sin \varphi_i - r_j \sin \varphi_j \right)$$

Finally, the intensity can be integrated over a large spherical surface to yield the spectral density of the sound power:

$$\frac{dW}{d\Gamma} = \pi^3 \left(\frac{u}{c_x} \right)^2 M^3 \left(\frac{\rho c_x{}^3 R^2}{1+\phi^2} \right) \left(\frac{R}{\Lambda_f} \right)^2 \left[1 - \left(\frac{r_h}{R} \right)^2 \right]^2 g(\Gamma) F_1 \left(\frac{R}{\Lambda_f}, kR \right) \quad (21)$$

where

$$F_1 \left(\frac{R}{\Lambda_f}, kR \right) = \int_0^{\pi/2} F \left(\theta, \frac{R}{\Lambda_f}, kR \right) \sin \theta \cos^2\theta \, d\theta$$

The function F_1 has been calculated numerically and is plotted in figure 10 for a range of values of kR and R/Λ_f.

As an example, the theory has been applied to the following case:

Rotor hub-to-tip radius ratio $\dfrac{r_h}{R} = 0.5$

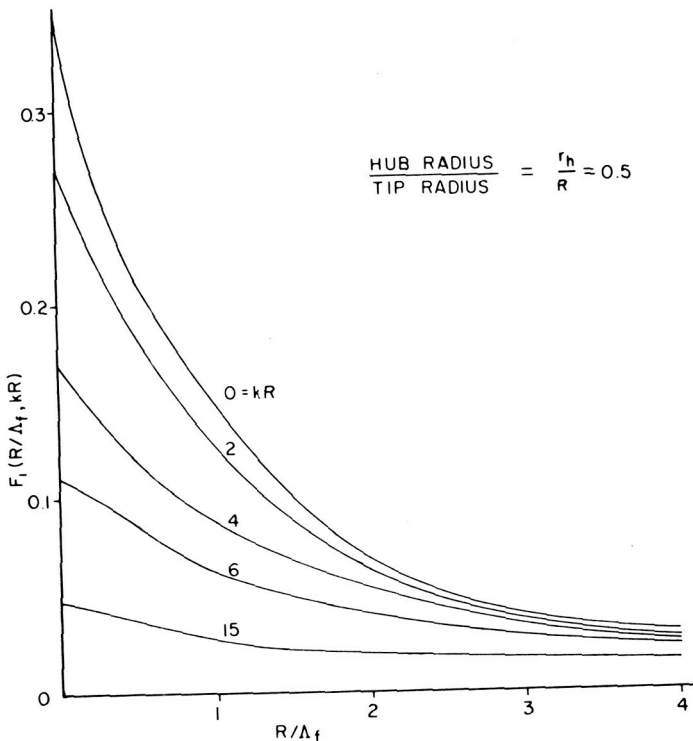FIGURE 10.—*Radiation function in the spectral density of the sound power.*

Flow coefficient $\phi = 0.64$

Axial flow Mach number $M = 0.25$

Ratio of integral scale to tip radius $\dfrac{\Lambda_f}{R} = 0.5$

This choice of Λ_f corresponds to the span of the blades. The resulting spectrum is shown in figure 11. The vertical scale is proportional to $\Gamma(dW/d\Gamma)$; i.e., a constant-percentage bandwidth, and the horizontal scale consists of the ratio of the integral scale Λ_f to the sound wavelength λ. The peak of the spectrum occurs at a value of $\Lambda_f/\lambda = 0.16$. The predicted spectrum level becomes inaccurate at values of $\Lambda_f/\lambda \geq 0.25$ since the integral scale of the turbulence and the wavelength of the sound become of comparable magnitude. A much more rapid, exponential decrease in the value of $\Gamma(dW/d\Gamma)$ than indicated in figure 11 would be expected.

The directivity of the sound pressure is illustrated in figure 12, which shows that the sound becomes progressively less directional as the integral scale Λ_f decreases.
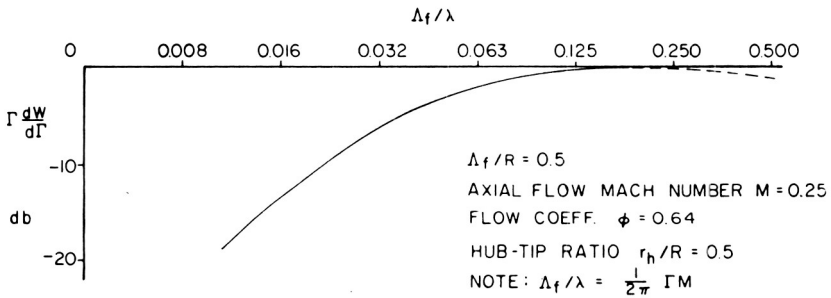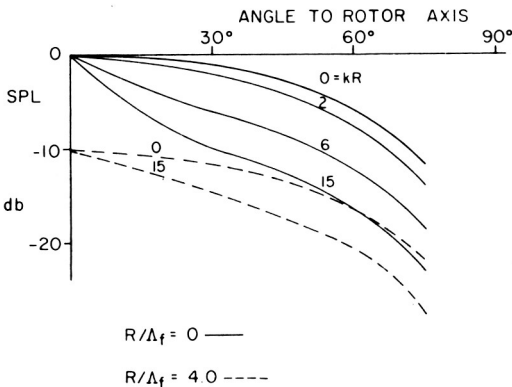

FIGURE 11.—*Broadband sound-power spectrum.*

FIGURE 12.—*Directivity of sound radiation.*

SUMMARY AND CONCLUSIONS

Broadband sound radiation from turbomachinery appears to be mainly due to turbulence in the approach stream. This turbulence may be generated by one of several mechanisms such as upstream blade rows or, in the case of turbines, the combustion system.

As a preliminary step in the calculation of the power spectral density of the radiated sound pressure, the spectrum tensor of the axial force fluctuations acting on a rotor have been found. These have been expressed in terms of aerodynamic response functions and the correlation tensor of the turbulence. At the present time, there is little information concerning the characteristics of the turbulence in turbomachinery. Also, expressions for the aerodynamic response functions are limited to two-dimensional, incompressible, thin-airfoil theory. Research in both areas is desirable. In order to make further progress and establish the general characteristics of the radiated sound, a simple case was considered. The turbulence in the approach stream was chosen to be isotropic and homogeneous, and the spectrum of the total force normal to a rotor disk was calculated. The predicted spectrum levels were compared with experimental results obtained on a 10-bladed propeller subjected to grid turbulence. Good agreement was observed.

The power spectral density of the sound intensity and of the sound power were next calculated. The spectrum depends on a number of parameters, such as the turbulence level, a characteristic time scale consisting of the ratio of the integral scale of the turbulence divided by the axial flow velocity, and characteristic length scales such as the ratio of the integral scale of the turbulence to the acoustic wavelength, the radius of the rotor, and the blade chord.

Due to the simplicity of the model used, only a limited number of cascade parameters enter the equations. In a more complete description, additional cascade parameters—such as the solidity and stagger angle—would also appear. As an example, the broadband sound-power spectrum for a turbomachinery rotor was calculated and plotted in figure 11. A flow coefficient of 0.64, a hub-to-tip ratio of 0.50, and an axial flow Mach number of 0.25 were chosen. The broadband sound power radiated has been estimated at 140 dB re 10^{-12} watts for a turbulence level of 5 percent of the axial velocity.

LIST OF SYMBOLS

B number of blades on rotor

$2b$ blade chord

C cascade parameter defined in equation (16)

c	speed of sound
c_x	axial flow velocity
e	cascade parameter defined in equation (16)
F	aerodynamic force function, defined in equation (1)
f	coefficient of longitudinal correlation of the turbulence
$G(\omega)$	spectrum function
$H(\omega)$	aerodynamic frequency response function
$K(\kappa)$	Sears function
k	acoustic wave number
ℓ	local lift force
M	Mach number of axial flow
n	number of blade elements
Q,Z	projections of q on the x and y axes, respectively
q	distance between blade elements
R	tip radius of rotor
r	distance, as variously defined
r_h	hub radius of rotor
t,T	time
U	tangential velocity of rotor
u	fluid velocity
W	sound power
w	flow velocity relative to the blades
$\mathbf{x},\mathbf{y}$	position vectors

Greek Letters

β	angle between the flow relative to the blade and the axial direction
Γ	frequency parameter, defined in equation (16)
Φ	correlation function
ϕ	flow coefficient, defined in equation (14)
κ	reduced frequency parameter in Sears function
Λ_f	integral length scale of the turbulence
λ	wavelength of the acoustic radiation
τ	time
θ,φ	position angles in polar coefficient
ω	angular frequency

APPENDIX: TABLE OF RADIATION FUNCTION[1]

$F(\theta, \frac{R}{\Lambda_f}, kR)$, defined by equation (20)

θ	kR	$\frac{R}{\Lambda_f} \rightarrow 0$	0.5	1.0	2.0	4.0
0°	0	1.0	0.620	0.408	0.208	0.088
	2	1.0	0.620	0.408	0.208	0.088
	4	1.0	0.620	0.408	0.208	0.088
	6	1.0	0.620	0.408	0.208	0.088
	15	1.0	0.620	0.408	0.208	0.088
30°	0	0.750	0.461	0.305	0.155	0.066
	2	0.640	0.410	0.275	0.145	0.064
	4	0.420	0.289	0.210	0.121	0.059
	6	0.250	0.194	0.151	0.100	0.054
	15	0.100	0.084	0.068	0.051	0.035
60°	0	0.250	0.155	0.101	0.052	0.022
	2	0.160	0.108	0.076	0.043	0.020
	4	0.071	0.055	0.044	0.031	0.017
	6	0.055	0.042	0.033	0.023	0.014
	15	0.022	0.017	0.014	0.011	0.008
90°	0	0	0	0	0	0
	2	0	0	0	0	0
	4	0	0	0	0	0
	6	0	0	0	0	0
	15	0	0	0	0	0

[1] This table applies to a hub/tip ratio of 0.50.

REFERENCES

1. BRAGG, S. L., AND R. BRIDGE, Noise from Turbojet Compressors. *J. Roy. Aeron. Soc.*, Vol. 68, No. 637, January 1964.

2. COPELAND, W. L., AND J. L. CRIGLER, *Noise Studies of Inlet-Guide-Vane—Rotor Interaction of a Single-Stage Axial-Flow Compressor.* NASA TN D-2962, September 1965.

3. SMITH, M. J. T., AND M. E. HOUSE, Internally Generated Noise from Gas Turbine Engines. Measurement and Prediction. *Trans. ASME, J. of Eng. Power*, April 1967, pp. 177–190.

4. SMITH, M. J. T., AND K. W. BUSHELL, *Turbine Noise—Its Significance in the Civil Aircraft Noise Problem.* ASME Paper 69–WA/GT–12, presented at the ASME Winter Annual Meeting (Los Angeles), November 16–20, 1969.

5. SHARLAND, I. J., Sources of Noise in Axial Flow Fans. *J. Sound Vib.*, Vol. 3, 1964, pp. 302–322.

6. TYLER, J. M., AND T. G. SOFRIN, Axial Flow Compressor Noise Studies. *Trans. SAE*, 1962, pp. 309–332.

7. MORFEY, C. L., *Sound Generation in Subsonic Turbomachinery.* ASME Paper 69–WA/FE–4, presented at the ASME Winter Annual Meeting (Los Angeles), November 16–20, 1969.

8. MANI, R., *Discrete Frequency Noise Generation From an Axial Flow Fan Blade Row.* ASME Paper 69–FE–12, presented at the ASME Applied Mechanics and Fluids Engineering Conference (Evanston, Ill.), June 16–18, 1969.

9. LIPSTEIN, N. J., AND R. MANI, *Experimental Investigation of Discrete Frequency Noise Generated by Unsteady Blade Forces.* ASME Paper 69–WA/FE–22, presented at the ASME Winter Annual Meeting (Los Angeles), November 16–20, 1969.

10. KRAMER, J. J., B. R. LEONARD, AND C. E. FEILER, *Low-Noise Propulsion Systems for Subsonic Transports.* ASME Paper 69–WA/GT–7, presented at the ASME Winter Annual Meeting (Los Angeles), November 16–20, 1969.

11. SEVIK, M., *The Response of Propulsors to Turbulence.* Presented at the 7th Symposium on Naval Hydrodynamics (Rome), 1968.

12. CURLE, N., The Influence of Solid Boundaries Upon Aerodynamic Sound. *Proc. Roy. Soc. (London)*, Series A, Vol. 231, 1955, pp. 505–514.

13. DOAK, P. E., Acoustic Radiation from a Turbulent Fluid Containing Foreign Bodies. *Proc. Roy. Soc. (London)*, Series A, Vol. 254, 1960, p. 129.

14. SEARS, W. R., Some Aspects of Non-Stationary Air Foil Theory and Its Practical Application. *J. Aeron. Sci.*, Vol. 8, No. 3, January 1941.

15. MORFEY, C. L., Broadband Sound Radiated from Subsonic Rotors. To be presented at the International Symposium on the Fluid Mechanics and Design of Turbomachinery (Penn State U.), August 31–September 3, 1970.

DISCUSSION

R. MANI (University of Massachusetts): It would seem from your description of the experimental apparatus that you have turbulence scales which are quite large compared to the propulsor size. It has been shown that you should get a predominance of blade-passage tones. If the eddies are really of substantial size, I do not really see how you would only get a broadband spectrum.

SEVIK (author): I believe that you are referring to a paper by Ffowcs Williams and Hawkings in which they show that blade-passage tones will also occur when the inflow is turbulent. They indicate that the bandwidth of the spectrum will be inversely proportional to the number of blades which are subject to the distortion field of a single eddy. Our test results do indeed show a "bump" around blade-passage frequency, which corresponds to their prediction. The bandwidth of the bump is about 40 cps, in agreement with their expression. Unfortunately, we also discovered after the tests that we had a blade resonance in the same frequency range and hence that there were two possible contributors to the energy. I agree that my theoretical approach does not predict the tones, but only the broadband energy.